

## Hard x-ray probe to study doping-dependent electron redistribution and strong covalency in $\text{La}_{1-x}\text{Sr}_{1+x}\text{MnO}_4$

J. Herrero-Martín, A. Mirone, J. Fernández-Rodríguez, and P. Glatzel  
*European Synchrotron Radiation Facility, F-38043 Grenoble Cedex 9, France*

J. García and J. Blasco  
*Instituto de Ciencia de Materiales de Aragón, CSIC-Universidad de Zaragoza, E-50009 Zaragoza, Spain*

J. Geck  
*IFW Dresden, P.O. Box 270116, D-01171 Dresden, Germany*

(Received 26 June 2009; revised manuscript received 22 January 2010; published 10 August 2010)

The doping dependence of the occupied  $3d$  states at the Mn sites of  $\text{La}_{1-x}\text{Sr}_{1+x}\text{MnO}_4$  ( $x=0, 0.3$ , and  $0.5$ ) was studied by means of nonresonant hard x-ray emission spectroscopy. For the single-crystalline samples, we observe a linear dichroism of the Mn  $K\beta$  main lines ( $3p$  to  $1s$  transitions) that is strongest for  $x=0$  and decreases with increasing hole doping  $x$ . At the same time, the Mn  $K\beta$  main lines of polycrystalline samples, i.e., the angular-integrated spectra, remain almost unchanged upon hole doping. The linear dichroism in the single crystals and the invariance of the  $K\beta$  lines in polycrystals lead to the conclusion that hole doping causes a spatial redistribution of the  $3d$  electrons without reducing the total charge and spin density at the manganese sites. This implies that the doped holes in  $\text{La}_{1-x}\text{Sr}_{1+x}\text{MnO}_4$  must have a strong oxygen  $2p$  character. Many-body cluster calculations are presented that support these findings.

DOI: [10.1103/PhysRevB.82.075112](https://doi.org/10.1103/PhysRevB.82.075112)

PACS number(s): 71.28.+d, 78.70.En, 71.10.-w, 75.47.Lx

### I. INTRODUCTION

The correlated electron systems realized in transition-metal oxide (TMO) materials attracted an enormous deal of attention due to their outstanding electronic properties. Most prominent examples are the high-temperature superconducting cuprates or the colossal magnetoresistive manganites. Conventional theoretical concepts often fail to explain the electronic properties of TMO materials. For instance, many of these compounds have a partially filled  $d$  shell but, at the same time, exhibit insulating ground states: a clear fingerprint of strong electronic correlations. Since a general theoretical treatment of electron correlations is currently beyond the available computing power, an essential step toward a better understanding of TMOs is the development of effective models, which retain only the most relevant electronic degrees of freedom, while still providing a realistic description.

In the case of the doped cuprates, it is now well established that such a model has to contain the Cu  $3d$  as well as the O  $2p$  bands. This is demonstrated by the fact that holes doped to the  $\text{CuO}_2$  planes are largely localized on the oxygen ligands, forming the famous Zhang-Rice singlet (ZRS) with the central Cu  $3d$  spin.<sup>1</sup> These ZRSs are an important concept to describe the complex charge dynamics in the doped cuprates.

For the doped manganites, the situation regarding the relevant electronic states is less clear: until recently, many studies did not consider the oxygen  $2p$  orbitals explicitly<sup>2-4</sup> while latterly others have highlighted the importance of the oxygen states.<sup>5-7</sup> In this paper, we address the issue of identifying the relevant electronic degrees of freedom for a prototypical manganite material, namely,  $\text{La}_{1-x}\text{Sr}_{1+x}\text{MnO}_4$ . These compounds, which are isostructural to high-

temperature superconducting  $\text{La}_{1-x}\text{Sr}_{1+x}\text{CuO}_4$ , do not show magnetoresistive behavior<sup>8</sup> but exhibit a wide range of electronic phases as a function of temperature and hole doping.<sup>9,10</sup>

The undoped parent compound  $\text{LaSrMnO}_4$  ( $x=0$ ) displays an antiferromagnetic and ferro-orbital ordered ground state.<sup>11</sup> It formally only contains high-spin  $\text{Mn}^{3+}$  sites ( $d^4$ ) coordinated by a distorted oxygen octahedron. According to an ionic picture, the distortion lifts the  $e_g$  degeneracy and stabilizes the  $3z^2-r^2$  orbital, which is singly occupied while the  $x^2-y^2$  level remains empty. However, since a half-filled  $d^5$  configuration is particularly stable, the ground state of such an octahedron is not a pure  $d^4$ , but has a large admixture of  $d^5\bar{L}$ , which already shows that the covalency between the transition metal and the oxygen ligands plays an important role.

Upon substitution of La by Sr in  $\text{La}_{1-x}\text{Sr}_{1+x}\text{MnO}_4$ , holes are doped into the system. This has a strong impact on the lattice structure, the electrical resistivity, and the magnetic properties.<sup>6</sup> In particular, a complex spin, charge, and orbital ordered ground states develops around  $x=0.5$  below 230 K. The charge order in this state was mostly discussed in terms of a checkerboard ordering of  $\text{Mn}^{3+}$  and  $\text{Mn}^{4+}$  sites.<sup>12</sup> However, such an integer charge segregation has been both experimentally<sup>13,14</sup> and theoretically<sup>15-17</sup> questioned. According to these studies, the spatial modulation of the manganese valence within the insulating and electronically ordered phase of half-doped  $\text{La}_{0.5}\text{Sr}_{1.5}\text{MnO}_4$  are very small, which would again point toward an active contribution of oxygen in the Mn-O bonding.

Experimentally, the doping-induced electronic changes can be examined in an element specific way by means of x-ray absorption spectroscopy (XAS), which probes the unoccupied states.<sup>18</sup> In the case of TMOs, the relevant valence

states can be accessed directly by measuring the transition metal  $L_{2,3}(2p \rightarrow 3d)$  and oxygen  $K(1s \rightarrow 2p)$  absorption edges in the soft x-ray range. Indeed, recent XAS and resonant soft x-ray scattering (RSXS) studies at the oxygen  $K$  edge do indicate that the O  $2p$  states play a prominent role in these materials.<sup>5-7</sup> In the hard x-ray region, the transition-metal  $K$  edges, where the main edge corresponds to  $1s \rightarrow 4p$  transitions, can be used to obtain information about the  $3d$  states. In this case, the  $3d$  states are probed indirectly via the  $4p$  states, which are also sensitive to structural distortions.

Complementary to probing the unoccupied states by XAS and related techniques such as RSXS,  $K$ -shell x-ray emission spectroscopy (XES) provides access to the occupied density of electronic states.<sup>19</sup> The  $K\beta$  main lines arise from intra-atomic  $3p$  to  $1s$  transitions. The hole in the  $3p$  shell in the final state of the transition strongly interacts with the valence electrons.<sup>20</sup> The  $(3p, 3d)$  exchange interaction splits the  $K\beta$  main lines into a sharp  $K\beta_{1,3}$  and a broad  $K\beta'$  feature.<sup>21,22</sup> The intra-atomic origin of the strongest interactions in the  $K\beta$  main lines is well established by comparison between spectra obtained on free metal atoms and solid-state systems.<sup>23</sup> Several studies of the  $K\beta$  lines in manganites have been reported previously.<sup>24-26</sup> The chemical sensitivity of the  $K\beta$  main lines arises from a modification of the  $(3p, 3d)$  interaction as a result of changes in the valence shell. The exchange interaction dominates and, for instance, a high-spin/low-spin transition has a very pronounced effect.<sup>27</sup> In the present case, where Mn is always in a high-spin configuration, a change in the Mn spin directly translates into a variation in the charge on the Mn.<sup>28</sup> Structural changes will only affect the  $K\beta$  line if they are accompanied by a change in the electronic structure that changes the  $(3p, 3d)$  interactions. A change in crystal-field splitting, for example, may barely modify the  $K\beta$  spectral shape as shown by Peng *et al.*<sup>28</sup>

In this paper, we report the  $K\beta$  main line spectra in polycrystalline and single-crystalline samples of  $\text{La}_{1-x}\text{Sr}_{1+x}\text{MnO}_4$  with  $x=0, 0.3, \text{ and } 0.5$  at room temperature. Many-body cluster calculations including the in-plane neighboring Mn sites are presented that successfully reproduce some of the experimental observations. The limitations of this approach are discussed.

## II. EXPERIMENTAL

Preparation of polycrystalline samples was done by solid-state reaction from the stoichiometric amounts of  $\text{La}_2\text{O}_3$ ,  $\text{SrCO}_3$ , and  $\text{MnCO}_3$ . The resulting powders were pressed into rods and sintered at  $1500^\circ\text{C}$  for 24 h in an oxygen atmosphere. Single crystals were grown from the rods by using a homemade floating-zone furnace as described in Ref. 13. They were cut with a surface normal to the  $[001]$  direction. Some pieces were ground and characterized by x-ray powder diffraction. All compounds exhibited patterns typical of a single phase. Magnetic characterization was also performed on these samples using a commercial Quantum Design superconducting quantum interference device magnetometer. The temperature scans of the dc magnetization for all

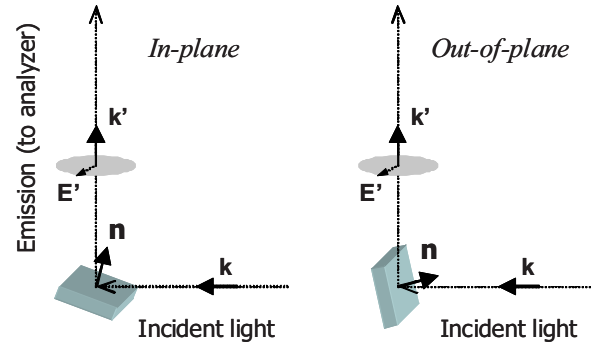


FIG. 1. (Color online) Geometry of the polarization-dependent XES measurements on single-crystalline samples in the  $\mathbf{k}' \sim \parallel \mathbf{n}$  (in-plane) and  $\mathbf{k}' \sim \perp \mathbf{n}$  (out-of-plane) configurations.  $\mathbf{E}'$  describes the electric vector of the nonpolarized emitted radiation. The crystal  $c$  axis coincides with  $\mathbf{n}$ .

samples were in agreement with the data reported in the literature.

X-ray emission spectra were recorded at beamline ID26 of the European Synchrotron Radiation Facility (ESRF) in Grenoble (France). The incident x rays were selected by means of a pair of cryogenically cooled Si (311) crystals. The total flux on the samples was  $5 \times 10^{12}$  photons/s. Non-resonant XES was performed at 6600 eV incident energy. The emission spectrometer employed one spherically bent ( $R=1$  m) Si crystal in (440) reflection that was arranged with sample and detector (avalanche photodiode) in a horizontal Rowland geometry at  $90^\circ$  scattering angle. All experiments were performed at room temperature. The beam size was  $0.3 \times 1$  mm<sup>2</sup> (horizontal  $\times$  vertical). A slit with 1.5 mm horizontal opening was placed in front of the detector. The energy bandwidth of the spectrometer was 0.6 (0.9 eV) eV at 6490 eV for the  $15^\circ$  ( $75^\circ$ ) geometry (*vide infra*). The influence of the change in spectral resolution on the measurements was tested by artificially broadening the spectra and forming difference spectra. It was found that the change in spectral broadening does not influence the results presented here. The step size for all recorded spectra was 0.2 eV. Three independent sets of data were recorded in order to determine the systematic experimental error to  $\sim 0.1$  eV.  $\text{LaMnO}_3$  and  $\text{CaMnO}_3$  were used as reference systems. The count rate in the maximum of the  $K\beta_{1,3}$  line is  $10^4$  counts/s.

The integral of the spectral area between 6465 and 6545 eV was normalized to one in all recorded emission spectra. The  $K\beta$  lines can be quantified either by a moment analysis of the  $K\beta_{1,3}$  line<sup>19</sup> or the integral of the absolute value of the difference (IAD).<sup>27</sup> The latter procedure proved to be more robust, i.e., less dependent on the spectral range, and was therefore chosen in the present study. The area below the emission curve of  $\text{LaMnO}_3$  was taken as a reference for the IAD analysis.

The geometry for the polarization-dependent study of the single-crystalline samples is shown in Fig. 1. We consider nonresonant x-ray emission where absorption and emission are not coherently coupled. The incident light is linearly polarized with the polarization in the plane that is spanned by  $(\mathbf{k}, \mathbf{k}')$ . The core hole has  $s$  (spherical) symmetry, the polarization of the incident x-ray beam is not relevant. The emit-

ted x rays with moment  $\mathbf{k}'$  form an angle  $(\mathbf{k}' \wedge \mathbf{c})$  of  $15^\circ$  ( $75^\circ$ ) with the  $c$  axis of the crystals unit cell. The error of this approximation to the 0 ( $90^\circ$ ) does not alter the conclusions in this work. We will refer to the two experimental geometries by  $\mathbf{k}' \sim \parallel \mathbf{n}$  ( $\mathbf{k}' \sim \perp \mathbf{n}$ ) throughout the paper. The crystal  $c$  axis coincides with the normal  $\mathbf{n}$  on the crystal surface.

We treat the emitted x rays within the dipole approximation. As a consequence, only  $3p_{x,y,z}$  orbitals that are normal to  $\mathbf{k}'$  are observed in  $3p$  to  $1s$  transitions in single crystals.<sup>19,29</sup> It follows that the  $\mathbf{k}' \sim \parallel \mathbf{n}$  geometry probes the crystal  $ab$ -plane components while  $\mathbf{k}' \sim \perp \mathbf{n}$  contains a 50% contribution from the crystals  $c$  axis.

### III. THEORY

We have simulated the effect of doping along the series using a many-body cluster model from a previous work<sup>16</sup> devoted to a RSXS study at the Mn  $L_{2,3}$  edge in  $\text{La}_{0.5}\text{Sr}_{1.5}\text{MnO}_4$ . In this model, the  $3d$  electrons of a central Mn site are coupled to the neighboring  $p$ -oxygen orbitals by a hopping term modulated by Slater-Koster parameters. Beyond the  $\text{MnO}_6$  octahedra, in-plane oxygen orbitals are in turn coupled to the orbitals of the neighboring Mn sites. To keep the Hilbert space dimension below an affordable limit, only one external  $e_g$  orbital per external Mn atom is considered: the one directed toward the central Mn. Different electronic configurations were considered while keeping constant the total number of electrons in the cluster, and limiting the oxidation state of the central Mn atom between +1 and +5. Using a larger number of configurations does not change the computed results. We have used our model to simulate the Mn  $3d$  occupancy as a function of doping and to simulate the Mn  $K\beta$  emission as well as its polarization dependence.

For the Mn  $3d$  occupancy study, we have kept the same set of parameters used for the fit of RSXS spectra in Ref. 16, except for  $\varepsilon_d$  in Eq. 5. This term determines the energy level of the external, i.e., nonphotoexcited, Mn  $3d$  orbitals and thus models in-plane oxygen mediated Mn-Mn interactions. By lowering (increasing) this level, we can increase (diminish) the electron occupancy on external orbitals. The external orbitals can hence be considered as a charge reservoir that allows to mimic the effect of doping on the  $\text{MnO}_6$  octahedra. Indeed, when  $\varepsilon_d$  increases (decreases), the ground-state energy is minimized by decreasing (increasing) the expectation value of electron occupancy on the external orbitals. As the total charge in the cluster is fixed, such doping affects the electron occupancies on the central Mn atom and on the six neighboring oxygen atoms.

To simulate the Mn  $K\beta$  emission and its polarization dependence, we have reset  $\varepsilon_d$  to its RSXS fit value, and added  $1s$  and  $3p$  shells to the model. Atomic values for the spin-orbit coupling  $\zeta_{3p}$  and the Slater integrals between  $3p$  and  $3d$  were calculated using Cowan's Hartree-Fock code.<sup>20</sup> These Slater integral values were then scaled down by a factor of 0.7. The renormalized Slater integrals  $F_{3p3d}^0$  and  $F_{1s3d}^0$  are both taken equal to  $1.1F_{dd}^0$ . The effect of the variation in the Mn-O apical distance as a function of doping was taken into account by rescaling the Mn-O hopping<sup>16</sup> for the apical bond. For the emission process, only the lowest energy con-

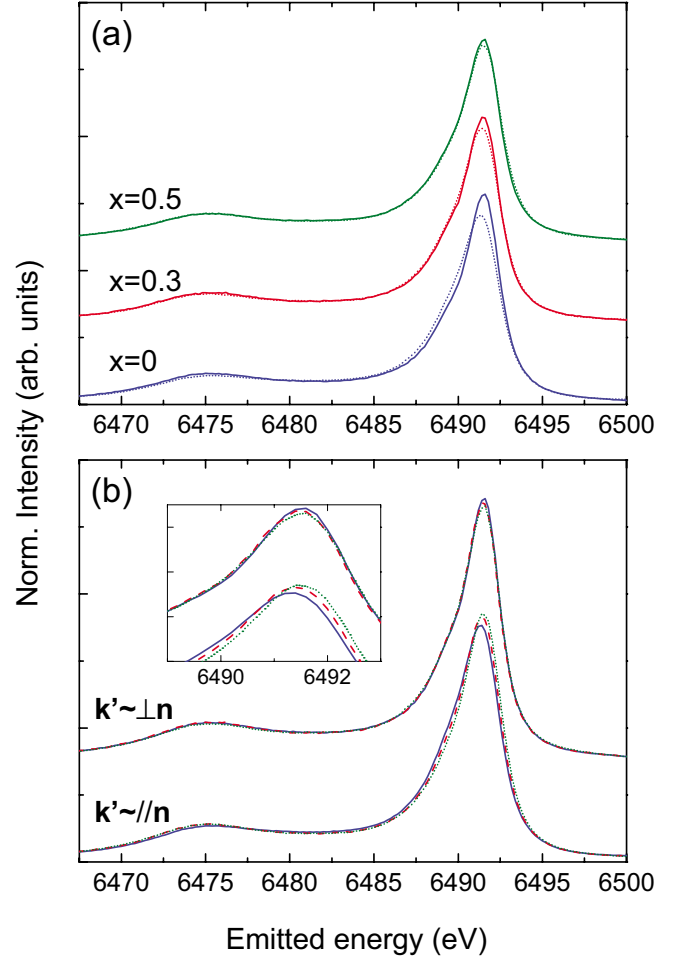


FIG. 2. (Color online)  $K\beta$  main emission from single crystals with doping  $x=0$  (blue), 0.3 (red), and 0.5 (green). The spectra are shown arranged by (a) compound, where solid and dotted lines refer to spectra recorded with  $\mathbf{k}' \sim \perp \mathbf{n}$  and  $\mathbf{k}' \sim \parallel \mathbf{n}$ , respectively, and by (b) geometry, where solid, dashed, and dotted lines correspond to  $x=0$ , 0.3, and 0.5 samples, respectively. The inset shows the maxima of the  $K\beta_{1,3}$  lines. The spectra have been shifted vertically for sake of clarity.

figurations of the system with one  $1s$  core hole were taken as initial states. Due to a weak  $1s$ - $3d$  coupling, these low-energy configurations correspond to differently coupled  $1s$ -shell and  $3d$ -shell spins. Higher energy configurations were not taken into account.<sup>21,30</sup>

In the calculation of the spectra, the final states in the region of the strong  $K\beta_{1,3}$  line (which corresponds to  $S=5/2$  in an ionic picture) were broadened with a Lorentzian function with width of 1.1 eV. For those corresponding to the  $K\beta'$  shoulder ( $S=3/2$ ), we used 4.4 eV. These values were adjusted in order to fit the data. The reason for the larger width observed for the  $S=3/2$  states resides in the fact that the  $3d$  to  $3p$  radiative decay channel is favored by the spin alignment of the  $3p$  hole with the  $3d$  spin.<sup>21-23</sup>

## IV. RESULTS AND ANALYSIS

### A. Single crystals

The experimental  $K\beta$  main emission lines from single crystals of  $\text{La}_{1-x}\text{Sr}_{1+x}\text{MnO}_4$  ( $x=0$ ,  $x=0.3$ , and  $x=0.5$ ) with

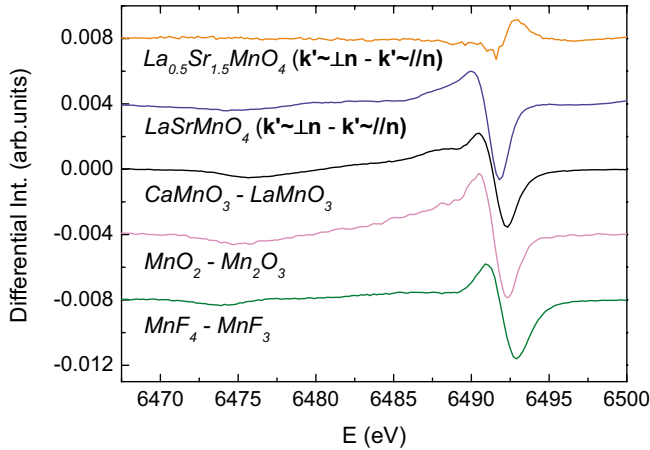


FIG. 3. (Color online)  $K\beta$  linear dichroism in  $\text{La}_{0.5}\text{Sr}_{1.5}\text{MnO}_4$  and  $\text{LaSrMnO}_4$  (top), compared to the  $K\beta$  difference spectrum of polycrystalline samples of references containing formal  $\text{Mn}^{\text{IV}}$  and  $\text{Mn}^{\text{III}}$ .

$\mathbf{k}' \sim \parallel \mathbf{n}$  and  $\mathbf{k}' \sim \perp \mathbf{n}$  are shown in Fig. 2. The  $K\beta$  spectrum is composed of the strong  $K\beta_{1,3}$  line at high energies and a broad  $K\beta'$  feature at lower energies. The linear dichroism in a single crystal is defined as the difference between the spectra for different polarizations, i.e., in the present case different angles between the crystal axes and the direction of the emitted x rays. The Mn-O distance along the  $c$  axis becomes considerably shorter ( $\sim 0.3$  Å) upon increasing  $x$  from 0 to 0.5 according to neutron powder and single-crystal diffraction as well as XAS studies while the average in-plane Mn-O bond length elongates by about one order of magnitude less.<sup>13,31</sup> The local geometry is tetragonally distorted for  $x=0$  and develops toward an octahedral coordination for  $x=0.5$ .<sup>6</sup> We find that the linear dichroism in the Mn x-ray emission is maximum for  $x=0$  and minimum for  $x=0.5$ . This corresponds to the evolution of the anisotropy of the local geometry. A linear dichroism has also been observed in the x-ray absorption  $K$  main edge<sup>13</sup> and the question arises whether the XES linear dichroism has its origin in the electronic structure or the local coordination. A very weak dichroism has been found in polarized XAS spectra for  $\text{La}_{0.5}\text{Sr}_{1.5}\text{MnO}_4$  at the Mn  $L_{2,3}$  edges.<sup>32</sup> The authors conclude that holes reside on hybrid states which are symmetric with respect to the  $a$  ( $b$ ) and  $c$  axis.

We show in Fig. 3 the difference spectrum between polycrystalline samples of the model systems  $\text{LaMn}^{\text{III}}\text{O}_3$  and  $\text{CaMn}^{\text{IV}}\text{O}_3$ . The differences between  $\text{Mn}_2^{\text{III}}\text{O}_3$  and  $\text{Mn}^{\text{IV}}\text{O}_2$  and between  $\text{Mn}^{\text{III}}\text{F}_3$  and  $\text{Mn}^{\text{IV}}\text{F}_4$  are also plotted as additional references. They have been taken from the  $K\beta$  emission line spectra in Ref. 19. The absolute energy calibration varies when comparing oxides, fluorides, and perovskites because the spectra were taken using different instruments. The relative energy calibration between  $\text{Mn}^{\text{III}}$  and  $\text{Mn}^{\text{IV}}$  systems, however, is correct because they were taken in the same experimental conditions. Thus the shape and not the position of the difference spectra can be compared. In all cases, the shift of the  $K\beta_{1,3}$  line with increasing oxidation state is accompanied by a decrease in the  $K\beta'$  intensity giving rise to a typical difference signal. Difference spectra be-

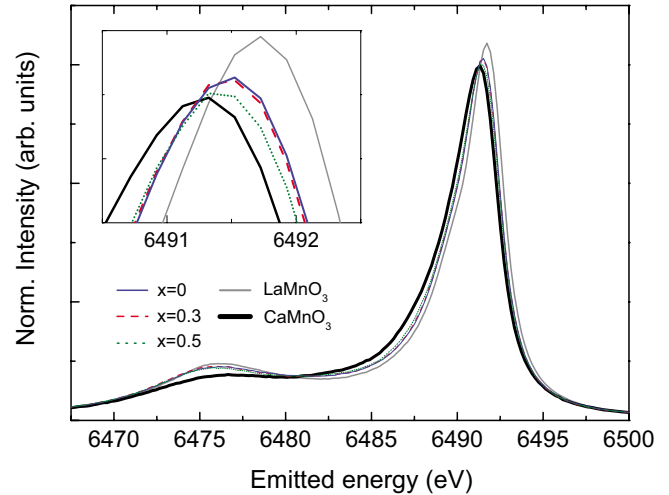


FIG. 4. (Color online) Mn  $K\beta$  main emission lines from polycrystalline samples of  $\text{La}_{1-x}\text{Sr}_x\text{MnO}_4$  for  $x=0$  (solid blue), 0.3 (dashed red), and 0.5 (dotted green). The spectra for  $\text{CaMnO}_3$  (thick black) and  $\text{LaMnO}_3$  (gray) are shown for comparison. The inset shows the maxima of the  $K\beta_{1,3}$  peak.

tween high-spin and low-spin Fe and Co systems have been reported by Vankó *et al.*<sup>27</sup> and Glatzel *et al.*<sup>33</sup> where a similar difference signal is observed. The strong similarity between the perovskites ( $\text{CaMn}^{\text{IV}}\text{O}_3$ - $\text{LaMn}^{\text{III}}\text{O}_3$ ), binary oxides, and fluorides difference curves compared to the linear dichroism for  $x=0$  suggests that the latter arises from a change in electronic structure, namely, a change in the valence-shell orbital population. Indeed, a decrease in  $3d$  orbital population results in a weaker  $K\beta'$  feature and a shift to lower energies of the  $K\beta_{1,3}$  peak.<sup>19,28</sup>

We thus find based on the linear dichroism that for the system with the strongest tetragonal distortion ( $x=0$ ) more electron density is present along the  $c$  direction than in the  $ab$  plane. This is readily understood since the  $3z^2-r^2$  orbital ( $\mathbf{z}$  coincides with  $c$  axis) is the first axial  $3d$  orbital that is populated in tetragonal symmetry with elongation along  $\mathbf{z}$  while the  $x^2-y^2$  orbital remains empty. The dichroic signal for  $x=0.5$  is small and the spectral shape markedly different. The signal is inverted as compared to the compounds with lower doping levels suggesting larger spin moment in the  $ab$  plane.

The changes in the  $K\beta$  main line along the doping series for the different polarizations [Fig. 2(b)] indicate an increase in electron density in the  $ab$  plane and a decrease along  $c$  with Sr doping. The angle-resolved emission spectra thus indicate that hole doping facilitates the charge transfer from the  $3z^2-r^2$  to the  $x^2-y^2$  orbitals as already proposed in Ref. 6 based on XAS and XRD measurements. It now needs to be determined by how much the integrated electron density in the Mn valence shell changes upon doping. To this end, the measurements on polycrystalline samples are discussed in the next section.

## B. Polycrystalline samples

The  $K\beta$  main emission spectra from polycrystalline samples of  $\text{LaSrMnO}_4$ ,  $\text{La}_{0.7}\text{Sr}_{1.3}\text{MnO}_4$ , and  $\text{La}_{0.5}\text{Sr}_{1.5}\text{MnO}_4$

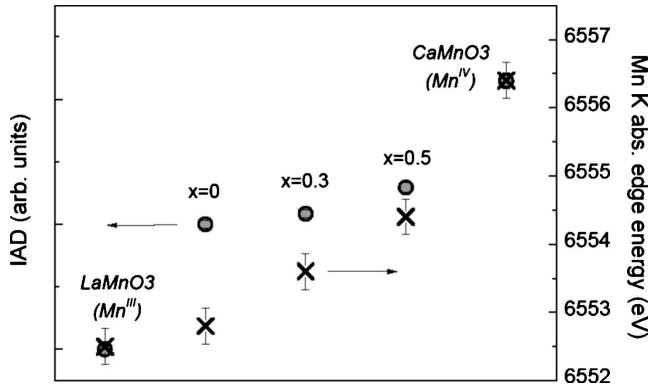


FIG. 5. Integrals of the absolute values of the difference spectra (IAD) for the Mn  $K\beta$  main emission lines from polycrystalline samples with  $x=0$ , 0.3, and 0.5, and  $\text{CaMnO}_3$  (circles) with  $\text{LaMnO}_3$  as reference. The energy position of the Mn  $K$  absorption spectra is shown along the right ordinate axis (crosses). The scale of the ordinate axes is chosen such that the IAD values and edge positions coincide for  $\text{LaMnO}_3$  and  $\text{CaMnO}_3$ .

are shown in Fig. 4 together with the reference systems  $\text{LaMnO}_3$  and  $\text{CaMnO}_3$ . The expected spectral change (*vide supra*) is observed between formal  $\text{Mn}^{\text{III}}$  in  $\text{LaMnO}_3$  and  $\text{Mn}^{\text{IV}}$  in  $\text{CaMnO}_3$ . We followed the procedure as suggested in Ref. 27 to quantify the spectral changes by means of the integrals of the absolute values of the difference spectra (IAD). The results are shown in Fig. 5.

Within a simple ionic picture, one would assign the spectral change from  $\text{LaMnO}_3$  to  $\text{CaMnO}_3$  to an integer decrease in charge on Mn. Formally, the spectral changes in the  $\text{La}_{1-x}\text{Sr}_{1+x}\text{MnO}_4$  series should span half of the change in the reference systems. This is based on the assumption that only Mn takes part in balancing of the charge upon hole doping. The charge on the oxygen ions is fixed at 2- in an ionic picture.

However, the Mn  $K\beta$  main line spectral shapes as well as the IAD values are nearly identical for the three samples of the  $\text{La}_{1-x}\text{Sr}_{1+x}\text{MnO}_4$  series. The change in IAD value between  $x=0$  and  $x=0.5$  is approximately 15% of the change between  $\text{LaMnO}_3$  and  $\text{CaMnO}_3$  as opposed to the expected 50%. The electronic structure at the Mn sites therefore changes much less than it would be anticipated based on an ionic model.

We also show in Fig. 5 the energy position of the Mn  $K$  main absorption edge (taken as the first maximum in the derivative of the absorption spectra) from the XANES measurements reported in Ref. 13 on polycrystalline samples of this series of compounds. The shifts of the main edge within the  $\text{La}_{1-x}\text{Sr}_{1+x}\text{MnO}_4$  series relative to the reference systems  $\text{LaMnO}_3$  and  $\text{CaMnO}_3$  are considerably larger than for the  $K\beta$  emission lines. While the  $K$ -edge position follows approximately what would be anticipated based on the formal valence, the spectral changes in the  $K\beta$  lines are substantially less than expected.

This apparent contradiction can be reconciled by noting that the  $K$  absorption edge is sensitive to both, the electronic structure and the local coordination while the  $K\beta$  lines are mainly sensitive to the electronic structure. We thus conclude

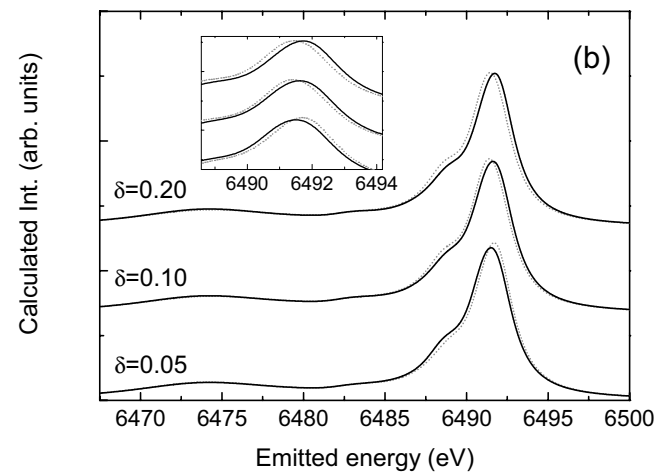
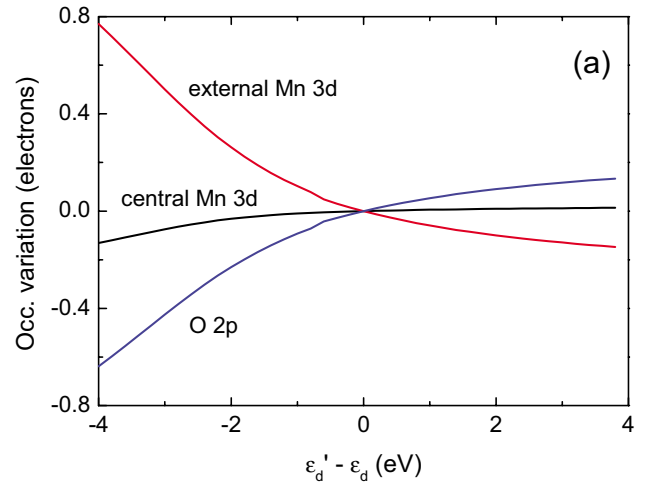


FIG. 6. (Color online) (a) Calculation of the occupancy variation for the  $3d$  shell of the central photoionized Mn and the  $2p$  states of the nearest six O as a function of the  $\epsilon'_d - \epsilon_d$  energy difference; (b)  $K\beta$  main emission lines calculated for  $\mathbf{k}' \sim \parallel \mathbf{n}$  (dotted gray) and  $\mathbf{k}' \sim \perp \mathbf{n}$  (solid black) as a function of the tetragonal distortion parameter  $\delta$  of the  $\text{MnO}_6$  octahedra.

that the edge shift in the  $\text{La}_{1-x}\text{Sr}_{1+x}\text{MnO}_4$  series mainly arises from changes in the interatomic distances and that the charge on the Mn ion changes only very little as evidenced by  $K\beta$  spectroscopy.

As a consequence, we find that the injected holes are mainly localized on the oxygen lattice as it was suggested by Ferrari *et al.*<sup>34</sup> We also point to the fact that the  $K\beta$  main line for  $\text{LaSrMnO}_4$  is already markedly different from  $\text{LaMnO}_3$  even though both compounds formally contain  $\text{Mn}^{\text{III}}$  ions. Layered and cubic structures thus give a different charge at the Mn site. In fact, Mn in  $\text{LaSrMnO}_4$  appears more oxidized than in  $\text{LaMnO}_3$ . We note that Tyson *et al.* invoked for the  $\text{LaMnO}_3$  and  $\text{CaMnO}_3$  reference systems a strong covalent character based on  $K\beta$  spectroscopy,<sup>35</sup> i.e., the difference in charge density on the Mn ions between the two systems is less than one electron.

X-ray emission lines that arise from transitions between core levels have been successfully modeled using ligand-field multiplet theory.<sup>18,19,28</sup> The reason for the good agreement between experiment and theory is that these deexcita-

tion processes are not directly sensitive to the fine structure of the energy levels in the valence shell. Correct treatment of the electron-electron interactions within an atomic multiplet model already provides good overall explanation of the spectral features. The influence of the valence electrons on the spectral shape is indirect via electron-electron interactions between the core hole and valence shell. Crystal-field splittings and orbital hybridizations may change the valence-shell electron configuration and thus influence the  $K\beta$  spectral shape. This can be considered in a ligand-field multiplet model as described in the following.

In Fig. 6(a), we show the occupancy variations for the central photoionized Mn  $3d$ , O  $2p$ , and external Mn  $3d$  orbitals as a function of the difference  $\varepsilon'_d - \varepsilon_d$  of the external Mn  $e_g$  energy with respect to the  $\varepsilon_d$  value established in Ref. 16. When the external orbital energy increases, electronic charge of these orbitals moves to the central  $\text{MnO}_6$  cluster. The cluster calculation shows that the central Mn  $3d$  occupancy variation is less than 0.1 electrons while the total charge on oxygen  $2p$  orbitals, in the  $\text{O}_6$  octahedra, varies by about 0.5 electrons. Our theoretical model therefore predicts that the effect of doping mainly affects the occupancy of oxygen orbitals while the variation in the charge on the Mn ions remains small. The model shows that holes are injected in Mn-O  $\sigma$  orbitals with a higher probability to find holes on oxygen atoms.

This behavior is due to the energy position of the oxygen bands relative to the Mn bands. We have done a numerical test, where we have “switched off” the Mn-O hopping term and kept the oxygen band filled and Mn in a  $3d^4$  configuration. Under these conditions, the energy of the filled oxygen band is  $\sim 0.7$  eV higher than the first unoccupied level on the Mn ion. This energy difference gets even larger in the intermediate state of the fluorescence process due to electron-hole interaction.

As an effect of hopping, ( $t=1.8$  eV) electrons are back-donated to Mn through the Mn-O bonds. The average back-donated charge is  $\sim 0.7$  electrons collectively given through all six bonds of the  $\text{MnO}_6$  octahedra. We have verified that the quantum numbers of the Mn ion remain almost constant under the effect of this backdonation. In particular,  $S^2$  is about 5.2, not far from 6, which is the Hund-rule predicted value for a  $3d^4$  electronic filling.

Figure 6(b) shows the calculated XES spectra for different values of the tetragonal distortions as described by  $\delta$ , where  $(1+\delta)$  is the ratio between  $c$  axis and in-plane Mn-O bond lengths. We have set equal distances for the  $a$  and  $b$  axes. In the model, we have rescaled the hopping parameters according to the length of the corresponding bonds, the scaling factor being  $(1+\delta)^{-3}$ . It can be observed that the anisotropy, in particular, the separation between the main peaks for in-plane and perpendicular polarizations, has the correct order of magnitude. We performed the same calculation for an isolated atom (setting the Mn-O hybridization to zero) and using a crystal field to remove the degeneracy in the  $3d$  orbitals (spectra not shown). This calculation strongly overestimates the linear dichroism and the agreement with experiment in this case is very poor.

The reason is that in the nonhybridized case, the  $3d_{3z^2-r^2}$  orbital has an occupation equal to one in the presence of a

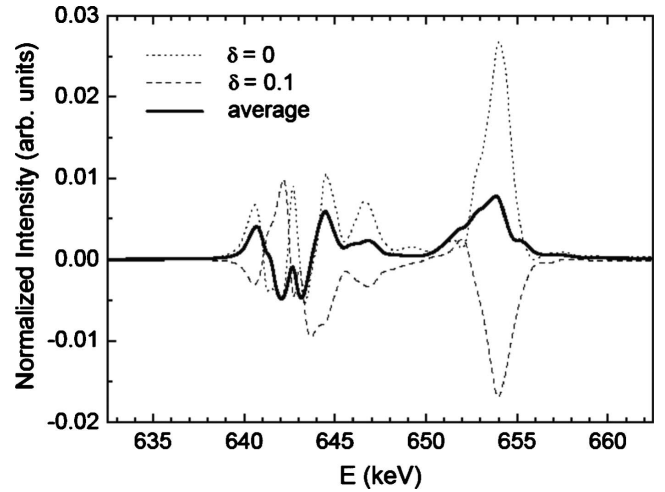


FIG. 7. Calculation of the x-ray absorption linear dichroism at the Mn  $L_{2,3}$  edges for a distorted  $\text{MnO}_6$  cluster with  $\delta=0$  (dotted line),  $\delta=0.1$  (dashed line), and the average of them (thick solid line).

crystal field while in the hybridized model, the occupation is less than one. This is due to the hopping between O and external orbitals, and between Mn and O. For the same reason, the  $3d_{x^2-y^2}$  occupation is nonzero in the presence of hybridization. Thus, orbital hybridization reduces the charge anisotropy around the Mn ion as compared to the ionic model. We define  $\delta$  as the difference between apical and basal Mn-O distances normalized by the average Mn-O bond length in each compound of the series. We observe that the linear dichroism has the correct sign for  $\delta=0.2$  (corresponding to  $\text{LaSrMnO}_4$ ) with the peak separation decreasing when  $\delta$  is reduced. This trend in the calculations is the result of the competition between two effects: first, the  $c$ -axis distortion which tends to increase the charge density along the  $c$  axis, and second, a kinetic effect which favors in-plane occupancy to lower the energy due to the oxygen-mediated hopping to external Mn orbitals. This conclusion is verified by a calculation for an isolated  $\text{MnO}_6$  octahedron where the external orbitals have been removed. In this case, the anisotropy is obtained immediately as soon as the octahedral symmetry is broken and remains practically independent of  $\delta$ . The model therefore implies that increase in the in-plane occupancy is related to intersite hopping processes within the  $ab$  plane.

Our calculations give, for  $\delta$  going to zero, a lower energy of the  $K\beta_{1,3}$  peak for  $\mathbf{k}' \sim \parallel \mathbf{n}$  than for  $\mathbf{k}' \sim \perp \mathbf{n}$  configuration. The experiment shows instead almost identical positions for the two peaks. We think that the reason for this discrepancy lies in the limited size of our model. In reality, the ground state in manganites is realized by a symmetry-broken phase which consists of different nonequivalent Mn sites, long-range ordered at low temperatures. We think that in the real system some of these sites conserve a charge anisotropy with more charge along the  $c$  axis which counterbalance the effect of those sites whose charge is reoriented into the  $ab$  plane by Mn-Mn interaction.

A more realistic calculation that takes a larger cluster into account may yield a better agreement. However, such calculations including all relevant interactions are beyond cur-

rently available computing power. A feasible approximation consists of performing separate calculations for the two Mn sites and average their contributions. We assume that inequivalent Mn sites can be characterized by different 3d-shell configurations: one shows an occupied in-plane  $e_g$  orbital while in the other site, the out-of-plane orbital is occupied. In the absence of distortion ( $\delta=0$ ), the first case is favored while a tetragonal distortion with  $\delta=0.1$  suffices to realize the latter configuration.

Another experimental technique that has been used to study the reorientation of the occupied  $e_g$  orbitals is XAS linear dichroism at the  $L$  edge. Huang *et al.*<sup>36</sup> observed that the occupied  $e_g$  orbitals, in  $\text{La}_{0.5}\text{Sr}_{1.5}\text{MnO}_4$  have a prevalent component along the  $c$  axis. In Fig. 7, we show our calculation for the XAS linear dichroism at the  $L_{2,3}$  edges for tetragonally distorted  $\text{MnO}_6$  clusters. The difference between the absorption for light polarization perpendicular and parallel to the  $c$  axis has been calculated for  $\delta=0$  and  $\delta=0.1$ . The average of these two calculations is also shown in the figure which corresponds to  $\text{La}_{0.5}\text{Sr}_{1.5}\text{MnO}_4$  ( $\delta=0.05$ ) where there are two nonequivalent Mn sites present. Here the calculated XAS linear dichroism has on average a positive component and it agrees reasonably well with the experimental data.<sup>36</sup>

## V. CONCLUSIONS

We have presented a  $K\beta$  study on polycrystalline and single-crystalline samples of the  $\text{La}_{1-x}\text{Sr}_{1+x}\text{MnO}_4$  series. The  $K\beta$  main emission lines from powders show that the electron density that is localized on the Mn atoms changes very little for  $0 \leq x \leq 0.5$ . This is not consistent with a change in the electron density by 0.5 electrons per Mn atom. A similar behavior had been reported in  $\text{La}_{1-y}\text{Ca}_y\text{MnO}_3$  for  $0 < y < 0.3$  where it was related to the transition from the insulator to conductive character of the samples that occurs in this doping range.<sup>35</sup> We explain our results with an active role of the neighboring O atoms in the charge-transfer process and an almost unchanged total Mn 3d occupancy.

In addition, the polarization-dependent measurements done on single crystals reveal that the main change related to

Mn 3d orbitals is a redistribution of the  $e_g$  charge from states oriented out-of-plane to states parallel to the  $ab$  plane.

These two main results, namely, (i) the small change in the charge on Mn upon increasing  $x$  and (ii) the redistribution of the  $e_g$  electrons have been reproduced by many-body cluster calculations. They yield a pronounced O 2p character of the doped charge carriers, which explains (i). Further, the extended cluster calculation evidences that the charge redistribution related to the  $e_g$  orbitals is mainly caused by non-local effects (kinetic energy, exchange interactions) within the  $ab$  planes.

These conclusions are in good agreement with a previous O  $K$  edge study,<sup>6</sup> where complementary results regarding the unoccupied O 2p states were reported.

Taken together the above discussion shows that the doping-induced changes to the electronic structure involve both the oxygen 2p and the Mn 3d bands, which both play an active role, and contrast with the classical ionic model perspective as previously stated.<sup>5,7,37,38</sup>

We believe that this result is an important input for the development of effective models which is an essential step toward a better understanding of these complex materials. Other theoretical approaches to the physics of manganites include recent local-density approximation plus dynamical mean field theory (DMFT) calculations that have led to promising results.<sup>39</sup> It would be interesting to apply this formalism to the series of compounds studied here and compare the results to our analysis of the experimental data.

## ACKNOWLEDGMENTS

We acknowledge the European Synchrotron Radiation Facility for provision of synchrotron radiation facilities and the financial support from Spanish MICINN, Project no. FIS2008-03951. J.G. acknowledges the German DFG through the Emmy-Noether Program, J. F.-R. the Gobierno del Principado de Asturias for the financial support from Plan de Ciencia, Tecnología e Innovación PCTI de Asturias 2006–2009.

<sup>1</sup>F. C. Zhang and T. M. Rice, *Phys. Rev. B* **37**, 3759 (1988).

<sup>2</sup>S. K. Mishra, R. Pandit, and S. Satpathy, *Phys. Rev. B* **56**, 2316 (1997).

<sup>3</sup>S. B. Wilkins, P. D. Spencer, P. D. Hatton, S. P. Collins, M. D. Roper, D. Prabhakaran, and A. T. Boothroyd, *Phys. Rev. Lett.* **91**, 167205 (2003).

<sup>4</sup>M. v. Zimmermann, J. P. Hill, D. Gibbs, M. Blume, D. Casa, B. Keimer, Y. Murakami, Y. Tomioka, and Y. Tokura, *Phys. Rev. Lett.* **83**, 4872 (1999).

<sup>5</sup>J. García, M. C. Sánchez, J. Blasco, G. Subías, and M. G. Proietti, *J. Phys.: Condens. Matter* **13**, 3243 (2001).

<sup>6</sup>M. Merz, G. Roth, P. Reutler, B. Büchner, D. Arena, J. Dvorak, Y. U. Idzerda, S. Tokumitsu, and S. Schuppler, *Phys. Rev. B* **74**, 184414 (2006).

<sup>7</sup>S. Grenier, K. J. Thomas, J. P. Hill, U. Staub, Y. Bodenthin, M.

García-Fernández, V. Scagnoli, V. Kiryukhin, S.-W. Cheong, B. G. Kim, and J. M. Tonnerre, *Phys. Rev. Lett.* **99**, 206403 (2007).

<sup>8</sup>Y. Moritomo, A. Asamitsu, H. Kuwahara, and Y. Tokura, *Nature (London)* **380**, 141 (1996).

<sup>9</sup>J.-C. Bouloux, J.-L. Soubeyroux, G. Le Flem, and P. Hagenmuller, *J. Solid State Chem.* **38**, 34 (1981).

<sup>10</sup>S. Larochele, A. Mehta, L. Lu, P. K. Mang, O. P. Vajk, N. Kaneko, J. W. Lynn, L. Zhou, and M. Greven, *Phys. Rev. B* **71**, 024435 (2005).

<sup>11</sup>W. B. Wu, D. J. Huang, G. Y. Guo, H.-J. Lin, T. Y. Hou, C. F. Chang, C. T. Chen, A. Fujimori, T. Kimura, H. B. Huang, A. Tanaka, and T. Jo, *J. Electron Spectrosc. Relat. Phenom.* **137-140**, 641 (2004).

<sup>12</sup>J. B. Goodenough, *Phys. Rev.* **100**, 564 (1955).

<sup>13</sup>J. Herrero-Martín, J. García, G. Subías, J. Blasco, and M. C.

- Sánchez, *Phys. Rev. B* **72**, 085106 (2005).
- <sup>14</sup>J. Herrero-Martín, J. García, G. Subías, J. Blasco, and M. C. Sánchez, *Phys. Rev. B* **70**, 024408 (2004).
- <sup>15</sup>T. Mizokawa and A. Fujimori, *Phys. Rev. B* **56**, R493 (1997).
- <sup>16</sup>A. Mirone, S. S. Dhesi, and G. Van der Laan, *Eur. Phys. J. B* **53**, 23 (2006).
- <sup>17</sup>C. Ma, H. X. Yang, L. J. Zeng, Z. A. Li, Y. Zhang, Y. B. Qin, and J. Q. Li, *J. Phys.: Condens. Matter* **21**, 045601 (2009).
- <sup>18</sup>F. M. F. de Groot and A. Kotani, *Core Level Spectroscopy of Solids* (Taylor & Francis, New York, 2008).
- <sup>19</sup>P. Glatzel and U. Bergmann, *Coord. Chem. Rev.* **249**, 65 (2005).
- <sup>20</sup>R. D. Cowan, *The Theory of Atomic Structure and Spectra* (University of California Press, Berkeley, 1981).
- <sup>21</sup>P. Glatzel, U. Bergmann, F. M. F. de Groot, and S. P. Cramer, *Phys. Rev. B* **64**, 045109 (2001); P. Glatzel, Ph.D. thesis, Hamburg University, 2001.
- <sup>22</sup>M. Taguchi, T. Uozumi, and A. Kotani, *J. Phys. Soc. Jpn.* **66**, 247 (1997).
- <sup>23</sup>A. von dem Borne, R. L. Johnson, B. Sonntag, M. Talkenberg, A. Verwey, Ph. Wernet, J. Schulz, K. Tiedtke, Ch. Gerth, B. Obst, and P. Zimmermann, and J. E. Hansen, *Phys. Rev. A* **62**, 052703 (2000).
- <sup>24</sup>J. Garcia, M. C. Sanchez, G. Subias, J. Blasco, and M. G. Proietti, *J. Synchrotron Radiat.* **8**, 892 (2001).
- <sup>25</sup>Q. Qian, T. A. Tyson, C.-C. Kao, M. Croft, S.-W. Cheong, G. Popov, and M. Greenblatt, *Phys. Rev. B* **64**, 024430 (2001).
- <sup>26</sup>H. Hayashi, M. Kawata, Y. Udagawa, N. Kawamura, and S. Nanao, *Phys. Rev. B* **70**, 134427 (2004).
- <sup>27</sup>G. Vankó, T. Neisius, G. Molnár, F. Renz, S. Kárpáti, A. Shukla, and F. M. F. de Groot, *J. Phys. Chem. B* **110**, 11647 (2006).
- <sup>28</sup>G. Peng, F. M. F. deGroot, K. Hiimiliinen, J. A. Moore, X. Wang, M. M. Grush, J. B. Hastings, D. P. Siddons, W. H. Armstrong, O. C. Mullins, and S. P. Cramer, *J. Am. Chem. Soc.* **116**, 2914 (1994).
- <sup>29</sup>U. Bergmann, J. Bendix, P. Glatzel, H. B. Gray, and S. P. Cramer, *J. Chem. Phys.* **116**, 2011 (2002).
- <sup>30</sup>We have only considered the fully relaxed eigenvectors and verified the validity of our approach by taking the lowest energy eigenvector of the nonionized system. The resulting vector projects to 90% over the two almost-degenerated lowest levels of the 1s core-hole system.
- <sup>31</sup>D. Senff, P. Reutler, M. Braden, O. Friedt, D. Bruns, A. Cousson, F. Bourée, M. Merz, B. Büchner, and A. Revcolevschi, *Phys. Rev. B* **71**, 024425 (2005).
- <sup>32</sup>M. Merz, P. Reutler, B. Büchner, D. Arena, J. Dvorak, Y. U. Idzerda, S. Tokumitsu, and S. Schuppler, *Eur. Phys. J. B* **51**, 315 (2006).
- <sup>33</sup>P. Glatzel, L. Jacquamet, U. Bergmann, F. M. F. de Groot, and S. P. Cramer, *Inorg. Chem.* **41**, 3121 (2002).
- <sup>34</sup>V. Ferrari, M. Towler, and P. B. Littlewood, *Phys. Rev. Lett.* **91**, 227202 (2003).
- <sup>35</sup>T. A. Tyson, Q. Qian, C. C. Kao, J. P. Rueff, F. M. F. de Groot, M. Croft, S. W. Cheong, M. Greenblatt, and M. A. Subramanian, *Phys. Rev. B* **60**, 4665 (1999).
- <sup>36</sup>D. J. Huang, W. B. Wu, G. Y. Guo, H.-J. Lin, T. Y. Hou, C. F. Chang, C. T. Chen, A. Fujimori, T. Kimura, H. B. Huang, A. Tanaka, and T. Jo, *Phys. Rev. Lett.* **92**, 087202 (2004).
- <sup>37</sup>J. C. Loudon, L. F. Kourkoutis, J. S. Ahn, C. L. Zhang, S.-W. Cheong, and D. A. Muller, *Phys. Rev. Lett.* **99**, 237205 (2007).
- <sup>38</sup>N. Mannella, C. H. Booth, A. Rosenhahn, B. C. Sell, A. Nambu, S. Marchesini, B. S. Mun, S.-H. Yang, M. Watanabe, K. Ibrahim, E. Arenholz, A. Young, J. Guo, Y. Tomioka, and C. S. Fadley, *Phys. Rev. B* **77**, 125134 (2008).
- <sup>39</sup>K. Held, O. K. Andersen, M. Feldbacher, A. Yamasaki, and Y.-F. Yang, *J. Phys.: Condens. Matter* **20**, 064202 (2008).